ELSEVIER

International Journal of Heat and Fluid Flow 22 (2001) 633–642

International Journal of HEAT AND FLUID FLOW

www.elsevier.com/locate/ijhff

Direct numerical simulation of the near field dynamics of a rectangular reactive plume

X. Jiang *, K.H. Luo

Department of Engineering, Queen Mary and Westfield College, University of London, Mile End Road, London E1 4NS, UK

Received 15 October 2000; accepted 21 June 2001

Abstract

Spatial direct numerical simulation (DNS) is used to study the near field dynamics of a buoyant diffusion flame established on a rectangular nozzle with an aspect ratio of 2:1. Combustion is represented by a one-step finite-rate Arrhenius chemistry. Without applying external perturbations at the inflow boundary, large vortical structures develop naturally in the flow field, which interact with the flame and temporally create localized holes within the reaction zone in which no chemical reactions take place. The interaction between density gradients and gravity plays a major role in the vorticity generation of the buoyant plume. At the downstream of the reactive plume, a more disorganized flow regime characterized by small scales has been observed, following the breakdown of the large vortical structures due to three-dimensional (3D) vortex interactions. Analysis of energy spectra shows that the spatially developing reactive plume has a tendency of transition to turbulence under the effects of combustion-induced buoyancy. The buoyancy effects are found to be very important to the formation, development, interaction, and breakdown of vortices in reactive plumes. In contrast with the relaminarization effects of chemical exothermicity *via* viscous damping and volumetric expansion on non-buoyant jet diffusion flames, the tendency towards transition to turbulence in reactive plumes is greatly enhanced by the buoyancy effects.

Keywords: DNS; Buoyancy; Transition; Combustion; Non-circular jets

1. Introduction

As an efficient technique of passive flow control, jets in non-circular configurations, such as elliptic, rectangular, square and triangular geometries, are encountered in various engineering applications such as combustors, cooling of energy conversion devices, and exhaust of aerospace vehicles. Non-circular jets have attracted an extensive research interest in recent years, both experimentally (e.g. Ho and Gutmark, 1987; Hertzberg and Ho, 1995; Zhang, 2000) and numerically (e.g. Miller and Madnia, 1995; Grinstein and Kailasanath, 1995; 1996; Grinstein and DeVore, 1996; Wilson and Demuren, 1998). Recently, the topic has been reviewed by Gutmark and Grinstein (1999).

In a broad range of practical applications, buoyancy due to density inhomogeneity under the influence of gravity plays a major role in the flow development of non-circular jets. The density inhomogeneity can result from inhomogeneities in temperature, differences in concentration of chemical species, changes in material phase, and many other effects in the flow field. Buoyancy effects are especially important to low-speed combustion applications, such as fires. However, buoyancy effects have not been taken into consideration in the existing numerical studies of non-circular jets (Miller and Madnia, 1995; Grinstein and Kailasanath, 1995, 1996; Grinstein and DeVore, 1996; Wilson and Demuren, 1998).

Free jets and plumes in open-boundary domains with buoyancy effects usually consist of a strongly buoyant near field and a turbulent, weakly buoyant far field. In the near field, the most prominent feature of buoyant jets and plumes is that the large vortical structures dominate the flow field of both reacting and non-reacting flows (e.g. Cetegen and Ahmed, 1993; Katta et al., 1994; Lingens et al., 1996; Cetegen et al., 1998; Maxworthy, 1999; Jiang and Luo, 2000a). The mechanism leading to the formation of these vortical structures is believed to be an absolute flow instability (Lingens et al., 1996; Maxworthy, 1999; Jiang and Luo, 2000c), which is different from that of non-buoyant jets. It was dentified (Jiang and Luo, 2000c) that the evolution of vortices in buoyant jets and plumes does not rely on the spatial amplification of external perturbations applied at the flow boundary but on the interactions between the density gradients and gravity.

The near field dynamics of buoyant jets and plumes, such as the formation and transport of vortices and laminar to turbulent flow transition, still has not been fully understood. In general, theoretical analysis is not able to deal with such complicated flow patterns. Experimental measurements of

* Corresponding author. Fax: +44-20-8983-3052.
E-mail address: x.jiang@qmw.ac.uk (X. Jiang).

0142-727X/01/$ - see front matter
PII: S0142-727X(01)00123-0

Notation

Da, Ze, T_f	Damköhler number, Zeldovich number, and flame temperature
e	internal energy per unit mass
E_T	total energy, $\rho[e + (u^2 + v^2 + w^2)/2]$
Fr	Froude number
$\mathbf{g}$	gravitational acceleration vector
L	length
M	Mach number
M_i, W_i	chemical symbol and molecular weight for species i
p	pressure
Pr	Prandtl number
$\mathbf{q}$	heat flux vector
Q_h	heat of combustion
Re	Reynolds number
Sc	Schmidt number
St	Strouhal number
t	time
T	temperature
u, v, w	velocity components in x, y, and z directions
$\mathbf{V}$	velocity vector
x, y, z	coordinates in the minor axis, major axis, and streamwise (vertical) directions
Y_i	mass fraction for species i

Greeks

γ	ratio of specific heats
μ	dynamic viscosity
v_i	stoichiometric coefficient for species i
ξ	mixture fraction
ρ	density
$\boldsymbol{\tau}$	viscous stress tensor
χ	scalar dissipation rate
$\boldsymbol{\omega}$	vorticity vector
ω_T	reaction rate

Other symbol

∇	gradient

Superscripts

$*$	dimensional quantities
T	transposition

Subscripts

0	fuel source
a	oxidant ambient
f, o, p	fuel, oxidizer and product
ref	reference

the flow field are difficult to reach a high level of detail and accuracy, especially for reacting flows. By using experimental techniques, it is also hard to investigate the mechanisms involved in the physical problem due to the coupling among combustion, buoyancy, and flow turbulence. For the study of the near field dynamics including flow transition, the conventional numerical simulations based on Reynolds averaging are not suitable either. Advanced numerical techniques, such as direct numerical simulation (DNS), provide a possibility to get a better understanding of the physical problem.

Numerical studies on buoyant jets and plumes in non-circular configurations especially those concerning combustion-induced buoyancy effects are very scarce in the literature. Previous studies on buoyant jets and plumes by the present authors (Jiang and Luo, 2000a,b,c) were limited to axisymmetric and planar configurations. However, three-dimensional effects are important in many applications and 3D simulations are essential to the understanding of flow transition. In this study, a fully 3D simulation is performed for a buoyant rectangular plume with an aspect ratio of 2:1. The plume considered is unsteady, viscous, reacting flow with temperature-dependent viscosity. A global, one-step reaction governed by temperature-dependent, finite-rate Arrhenius kinetics is used to represent the chemistry.

In the context of DNS, most simulations reported in the literature are temporal simulations (Moin and Mahesh, 1998) with the imposition of periodic boundaries in at least one direction, which are computationally less demanding. However, it is not possible to simulate buoyant non-circular jets and plumes in a temporal way because the buoyancy acceleration in the streamwise direction and the non-parallel effects due to flow entrainment through the side boundaries are significant in the near field. Therefore, a spatial DNS is necessary to simulate buoyant jets and plumes. To restrict the computational costs, the spatial DNS in this study is focused on the near field of the rectangular plume, which provides detailed information about the early stage of the spatial development of the flow field.

DNS results are presented mainly for a rectangular reactive plume in this paper, but some results from the simulation of a rectangular non-reactive thermal plume are also included to highlight their differences. The rest of the paper is organized as follows. Section 2 first presents the governing equations for the flow field, and then introduces the numerical methods and boundary conditions for the spatial DNS of open-boundary buoyant flows. Section 3 is a discussion of the simulation results from a comparative study of rectangular reactive and non-reactive plumes. The analysis of results is based on both instantaneous and time-averaged flow quantities. Finally, conclusions are drawn in Section 4.

2. Mathematical formulation

2.1. Governing equations

The physical problem is a fuel jet issuing vertically into an oxidant ambient environment. The aspect ratio of the rectangular nozzle was chosen to be 2:1, which is of practical interest (Hertzberg and Ho, 1995; Wilson and Demuren, 1998). The fuel and oxidizer are assumed to be unmixed at the base plane and a non-premixed flame is established above the rectangular base when the fuel/oxidizer mixing takes place. Currently, a complete DNS of reacting flows in 3D with multi-species transport and detailed chemistry is still out of reach of the computer power (Candel et al., 1999). In this investigation, a simple one-step global reaction $v_f M_f + v_o M_o \rightarrow v_p M_p$ with finite-rate Arrhenius kinetics is presumed for the chemistry to avoid the prohibitively high computational costs of a simulation with detailed chemistry.

The flow field is described as unsteady, buoyant, reacting flow with temperature-dependent viscosity. For the mathematical formulation of low-speed reacting flows, a low Mach number approximation to the governing equations is widely used to allow larger time steps compared with using the fully compressible formulation. However, in a DNS of reacting flows, it is usually the fastest reaction, and not the flow velocity

or acoustics, that sets the maximum allowable time steps. Therefore, the governing equations used in this study are the compressible time-dependent Navier–Stokes equations in non-dimensional form. The reaction rate is described by the Arrhenius law (Luo and Bray, 1998; Luo, 1999), which takes the form of $\omega_T = Da(\rho Y_f/W_f)^{\nu_f}(\rho Y_o/W_o)^{\nu_o}\exp[-Ze(1/T-1/T_f)]$ after normalization. It follows that the reaction rates for individual species are $\omega_f = -\nu_f W_f \omega_T$, $\omega_o = -\nu_o W_o \omega_T$ and $\omega_p = \nu_p W_p \omega_T$, respectively. The heat release rate is $\omega_h = Q_h \omega_T$. Reference quantities are: $g^*_{ref} = 9.81\ \mathrm{m/s^2}$, magnitude of the gravitational acceleration; $L^*_{ref} = L^*_0$, width of the fuel jet along the major axis direction at the inlet; $T^*_{ref} = T^*_a$, ambient temperature; $w^*_{ref} = w^*_0$, maximum streamwise (vertical direction) velocity of the fuel jet at the inlet; $\mu^*_{ref} = \mu^*_a$, fuel viscosity at ambient temperature; and $\rho^*_{ref} = \rho^*_a$, fuel density at ambient temperature. The dynamic viscosity was chosen to be temperature-dependent according to a power law of the form $\mu = \mu_a(T/T_a)^{0.76}$. The conservation laws for mass, momentum, energy and chemical species can be written in non-dimensional form as

$$\frac{\partial \mathbf{U}}{\partial t} + \frac{\partial \mathbf{E}}{\partial x} + \frac{\partial \mathbf{F}}{\partial y} + \frac{\partial \mathbf{G}}{\partial z} + \mathbf{S} = 0, \tag{1}$$

where the vectors $\mathbf{U}, \mathbf{E}, \mathbf{F}, \mathbf{G}$ and $\mathbf{S}$ are defined as $\mathbf{U} = (\rho, \rho u, \rho v, \rho w, E_T, \rho Y_f, \rho Y_o)^T$,

$$\mathbf{E} = \begin{bmatrix} \rho u \\ \rho u^2 + p - \tau_{xx} \\ \rho uv - \tau_{xy} \\ \rho uw - \tau_{xz} \\ (E_T + p)u + q_x - u\tau_{xx} - v\tau_{xy} - w\tau_{xz} \\ \rho uY_f - \frac{1}{ReSc}\left(\mu \frac{\partial Y_f}{\partial x}\right) \\ \rho uY_o - \frac{1}{ReSc}\left(\mu \frac{\partial Y_o}{\partial x}\right) \end{bmatrix},$$

$$\mathbf{F} = \begin{bmatrix} \rho v \\ \rho uv - \tau_{xy} \\ \rho v^2 + p - \tau_{yy} \\ \rho vw - \tau_{yz} \\ (E_T + p)v + q_y - u\tau_{xy} - v\tau_{yy} - w\tau_{yz} \\ \rho vY_f - \frac{1}{Re\,Sc}\left(\mu \frac{\partial Y_f}{\partial y}\right) \\ \rho vY_o - \frac{1}{Re\,Sc}\left(\mu \frac{\partial Y_o}{\partial y}\right) \end{bmatrix},$$

$$\mathbf{G} = \begin{bmatrix} \rho w \\ \rho uw - \tau_{xz} \\ \rho vw - \tau_{yz} \\ \rho w^2 + p - \tau_{zz} \\ (E_T + p)w + q_z - u\tau_{xz} - v\tau_{yz} - w\tau_{zz} \\ \rho wY_f - \frac{1}{Re\,Sc}(\mu \frac{\partial Y_f}{\partial z}) \\ \rho wY_o - \frac{1}{Re\,Sc}(\mu \frac{\partial Y_o}{\partial z}) \end{bmatrix},$$

$$\mathbf{S} = \begin{bmatrix} 0 \\ 0 \\ 0 \\ \frac{(\rho_a - \rho)g_z}{Fr} \\ \frac{(\rho_a - \rho)wg_z}{Fr} - \omega_h \\ -\omega_f \\ -\omega_o \end{bmatrix}.$$

Buoyancy terms are included in both the streamwise momentum and energy equations as $(\rho_a - \rho)g_z/Fr$ and $(\rho_a - \rho)wg_z/Fr$, where $g_z = -1$ is the gravity imposed in the downwards vertical direction. In the above governing equations, x-direction is aligned with the minor axis at the inlet, while y-coordinate is along the major axis. The terms "major" and "minor" used here refer to the dimensions of the fuel jet at the inlet plane. The constitutive relations for viscous stress components are

$$\tau_{xx} = -2/3\ \mu/Re\ (-2\partial u/\partial x + \partial v/\partial y + \partial w/\partial z),$$
$$\tau_{yy} = -2/3\ \mu/Re\ (\partial u/\partial x - 2\partial v/\partial y + \partial w/\partial z),$$
$$\tau_{zz} = -2/3\ \mu/Re\ (\partial u/\partial x + \partial v/\partial y - 2\partial w/\partial z),$$
$$\tau_{xy} = \mu/Re\ (\partial v/\partial x + \partial u/\partial y),$$
$$\tau_{xz} = \mu/Re\ (\partial w/\partial x + \partial u/\partial z),$$
$$\tau_{yz} = \mu/Re\ (\partial w/\partial y + \partial v/\partial z),$$

while the heat flux components are expressed as

$$q_x = -\mu/[(\gamma - 1)M^2 PrRe]\partial T/\partial x,$$
$$q_y = -\mu/[(\gamma - 1)M^2 PrRe]\partial T/\partial y,$$
$$q_z = -\mu/[(\gamma - 1)M^2 PrRe]\partial T/\partial z.$$

The perfect-gas law for the mixture is

$$p = \frac{\rho T}{\gamma M^2}\left(Y_f + \frac{W_f}{W_o}Y_o + \frac{W_f}{W_p}Y_p\right). \tag{2}$$

2.2. Numerical solution

The governing equations are solved using a sixth-order compact finite difference scheme with a spectral-like resolution (Lele, 1992) for the evaluation of the spatial derivatives in all the three directions. This allows more flexibility in the specification of boundary conditions (Jiang and Luo, 2000a,b), with minimal loss of accuracy relative to spectral methods. A third-order fully-explicit compact-storage Runge–Kutta scheme (Williamson, 1980) is used to advance the equations in time. The time step is limited by the Courant–Friedrichs–Lewy (CFL) condition for stability and a chemical restraint (an increase in the local product mass fraction of more than 0.01% is not allowed for one time step).

At the inlet, a rectangular plume source (fuel) with dimensions of (0∼0.5, −0.5∼0.5) is prescribed on the base plane of $0 \leqslant x \leqslant L_x$ and $-L_y/2 \leqslant y \leqslant L_y/2$, where L_x and L_y stand for the inlet domain size. For the streamwise velocity, a "top-hat" profile given by

$$w = \{1 + \tanh[20(0.5 - |x - L_x/2|)]\}\{1 + \tanh[20(1 - |y|)]\} / [1 + \tanh(10) + \tanh(20) + \tanh(10)\tanh(20)]$$

is assumed. At this base plane, the cross-stream velocity components are specified as zero. Therefore the flow initially has zero streamwise vorticity. The flow field inside the domain is initialized with the inlet conditions at the plume base. Buoyant jets and plumes display an intrinsic, absolutely unstable flow instability (Huerre and Monkewitz, 1990; Lingens et al., 1996; Maxworthy, 1999) in which vortices evolve naturally in the flow field due to the gravitational effects (Jiang and Luo, 2000c). Therefore there is no need to apply external perturbations at the inflow boundary for the development of flow vortices. In the numerical simulation, the external stimulus to initiate flow vortices can arise from a slight mismatch between the imposed initial conditions and solutions to the flow field. As a result of the spatial nature of the simulation, initial conditions are of minor importance to the developed flow field at the later stage.

Boundary conditions are specified using the general formulation for DNS of Navier–Stokes equations by Poinsot and Lele (1992), which is based on the analysis of characteristics. The computational domain is bounded by the inflow and outflow boundaries in the streamwise direction. At the inflow boundary, temperature is treated as a "soft" variable while

other variables are imposed with their initial values. For the outflow boundary, non-reflecting characteristic boundary condition (Thompson, 1987) is used. Such a boundary condition, like all others, assumes that the flow is 1D at the boundary. However, the real flow field at the outlet is of multi-dimensional nature due to the existence of flow vortices. It was found necessary to use an additional sponge layer (Jiang and Luo, 2000a,b) next to the outflow boundary to completely eliminate spurious wave reflections. The computational results in the sponge layer are not truly physical and therefore not used in the data analysis. The boundary condition in the cross-stream directions is the entrainment boundary condition (Jiang and Luo, 2000a,b), which allows entrainment of the ambient fluid into the computational domain with the entrainment velocity obtained from the characteristic form of the momentum equation by applying the local 1D inviscid relations (Poinsot and Lele, 1992). Details of the boundary conditions for the spatially developing open-boundary buoyant flow can be found in Jiang and Luo (2000a,b).

3. Results and discussion

Simulation results from a reacting case with $Re = 1000$ and $Fr = 1.5$ are presented. The effect of buoyancy on the resolution sets a limit on the Froude number that can be prescribed in DNS (Elghobashi et al., 1999) under a certain number of grid points. The Froude number used in this study was chosen so that the buoyant reacting flow field can be fully resolved. The fuel temperature at the inlet is assumed to be 3, which was chosen to ensure autoignition of the mixture (Grinstein and Kailasanath, 1995, 1996; Vervisch and Poinsot, 1998). To isolate the effects of combustion-induced buoyancy, the fuel and oxidizer are assumed to be of equal molecular weight. The ratio of specific heats, Prandtl and Schmidt numbers are assumed to be constants: $\gamma = 1.4$, $Pr = 1$ and $Sc = 1$. A Mach number $M = 0.1$ is used, under which the flow compressibility is negligible. The parameters used for the chemical reaction are: $Da = 6$, $Ze = 12$, $T_f = 6$, and $Q_h = 1650$. The reason behind the choice of these values is to mimic the behavior of a low heat release combustion within the computational restrictions.

A computational domain of the size of $3 \times 6 \times 8$ with a sponge layer above $z = 7$ is used, which was chosen to ensure a minimal effect of boundaries on the simulation results. The results presented next are obtained from a grid of $108 \times 216 \times 288$ nodes. For a sufficiently small reference length scale (e.g. $L^*_{ref} \leqslant 1$ cm), the grid points used are sufficient to fully resolve the energy spectrum. The results are considered to be grid-independent since no appreciable changes in the solution was observed when the grid spacing was decreased. The solution was also tested to be time step independent. Simulations have been performed on the massively parallel computer Cray T3E-1200E in Manchester by using 72 processors. The CPU time used for the reactive case is approximately 24000 PE hours, while it is about 9000 PE hours for the non-reactive case. The 3D parallel DNS code used in this study is an extension of the axisymmetric and planar DNS codes for buoyant reacting flows (Jiang and Luo, 2000a,b,c). In the following, results are mainly discussed for the reacting case, while some results from the non-reactive thermal plume simulation are also included to illustrate the effects of chemical heat release on the reactive plume.

3.1. Instantaneous plume structures

Buoyant jets and plumes display a periodic pulsation behavior known as "flickering" or "puffing" phenomenon associated with the formation and convection of buoyancy-induced large vortical structures in the near field (Cetegen and Ahmed, 1993; Katta et al., 1994; Lingens et al., 1996; Cetegen et al., 1998; Maxworthy, 1999; Jiang and Luo, 2000a). Fig. 1 shows the temperature contours on the major axis plane of the rectangular reactive plume at two different times within one pulsation period. It can be observed that large vortical structures evolve spatially in the flow field. Very close to the plume base, the "necking" phenomenon can be seen clearly, which is due to the buoyancy acceleration and flow entrainment (Jiang and Luo, 2000a). With the convection of the large vortical structures in the streamwise direction by the mean flow, the flow exhibits a periodic behavior. The pulsation period of this reactive plume is approximately $\Delta t = 2.0$. The maximum flame temperature at a certain location of the flow field also changes with time due to the periodic pulsation of the flow.

Fig. 2 shows the temperature contours on $z = 5.0$ plane at the downstream of the rectangular reactive plume. It can be observed that the local plume structure does not preserve its original rectangular shape. Due to the vortex deformation effects associated with the aspect ratio and corner features of the rectangular geometry (Wilson and Demuren, 1998; Gutmark

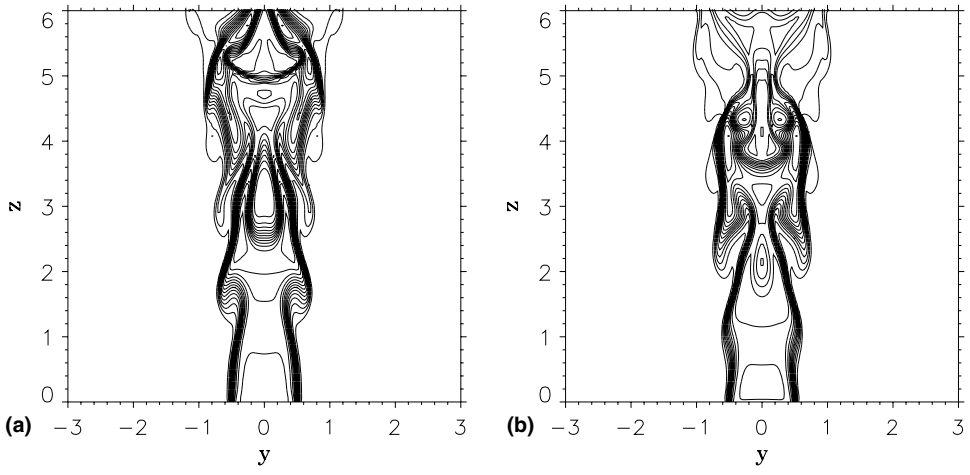

Fig. 1. Temperature contours on the major axis plane of the reactive plume (15 contours between the minimum and maximum as indicated): (a) 1.00–4.14 ($t = 23.0$); (b) 1.00–4.43 ($t = 24.0$).

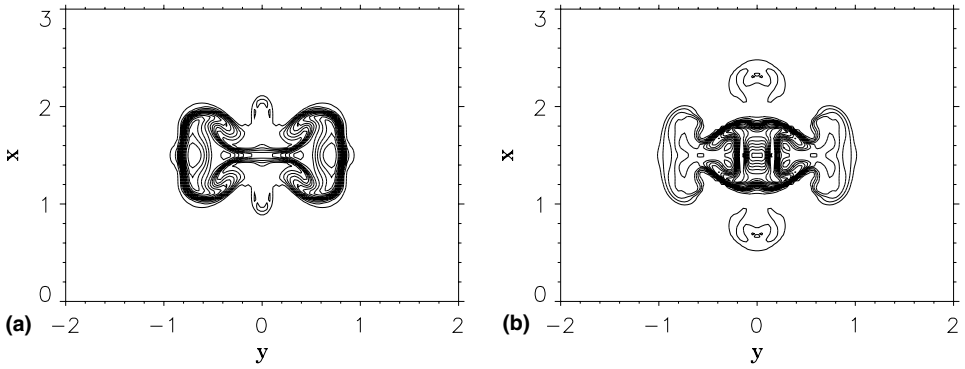

Fig. 2. Temperature contours on $z = 5.0$ plane of the reactive plume (15 contours between the minimum and maximum as indicated): (a) 1.00–3.88 ($t = 23.0$); (b) 1.00–2.73 ($t = 24.0$).

and Grinstein, 1999), the reactive plume evolves spatially with complex 3D structures.

Fig. 3 shows the temperature contours on the minor axis plane of the rectangular reactive plume. It is observed that the plume spreads rapidly in the minor axis direction at the downstream. The temperature contours of the non-reactive thermal plume on the minor axis plane corresponding to Fig. 3 are shown in Fig. 4. Apparently the thermal plume is much less vortical than the reactive plume and it does not spread significantly in the lateral direction. Although vortical structures start to form in the flow field and the flow exhibits a similar periodic behavior, the non-reactive thermal plume remains laminar without any significant spreading in the cross-streamwise directions. This behavior is similar to that observed in experiments for low density ratio plume with weak buoyancy (e.g. Cetegen et al., 1998).

The results discussed above clearly indicate the importance of combustion-induced buoyancy effects on the flow structures. The density ratio of the reactive plume is higher than that of the non-reactive thermal plume due to the chemical heat release. This difference in buoyancy level consequently leads to significant differences in the flow dynamics of the two cases. The differences between these two cases will be further discussed in terms of flow transition characteristics.

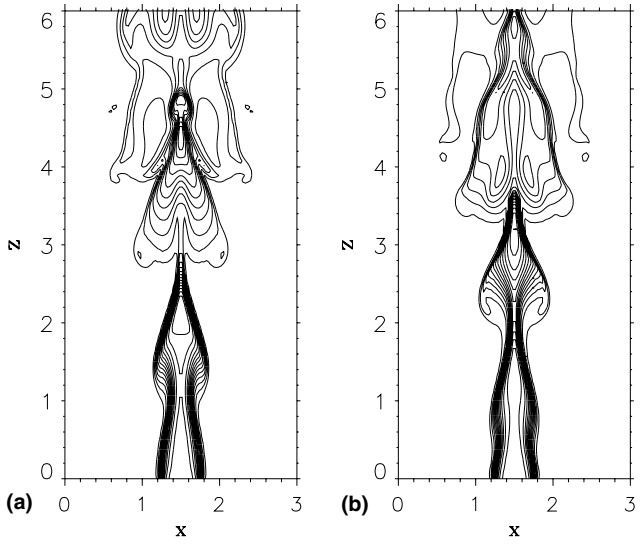

Fig. 3. Temperature contours on the minor axis plane of the reactive plume (15 contours between the minimum and maximum as indicated): (a) 1.00–3.86 ($t = 23.0$); (b) 1.00–3.86 ($t = 24.0$).

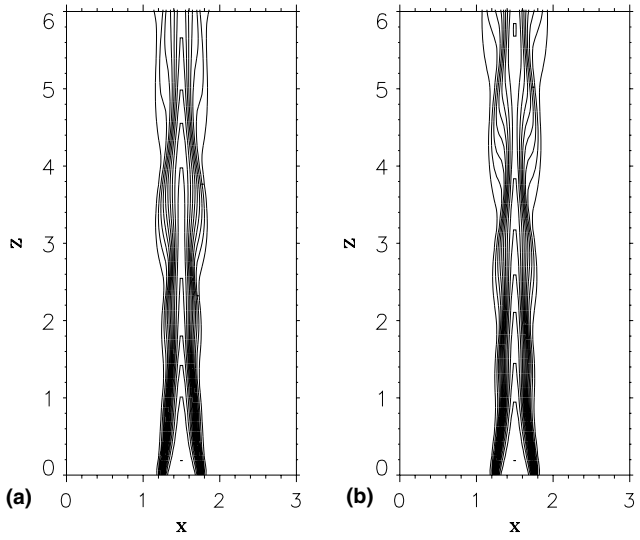

Fig. 4. Temperature contours on the minor axis plane of the non-reactive thermal plume (15 contours between the minimum and maximum as indicated): (a) 1.00–2.99 ($t = 23.0$); (b) 1.00–2.99 ($t = 24.0$);

For the reactive plume, combustion-induced vortices dominate the flow field. The 3D vortical structures in the reactive plume can be represented by distributions of the vorticity magnitude. The three components of the vorticity are $\omega_x = \partial w/\partial y - \partial v/\partial z$, $\omega_y = \partial u/\partial z - \partial w/\partial x$, and $\omega_z = \partial v/\partial x - \partial u/\partial y$, respectively. The 3D visualization of the enstrophy $(\omega_x^2 + \omega_y^2 + \omega_z^2)/2$, which is the magnitude of vorticity (Elghobashi et al., 1999) is shown in Fig. 5. It can be observed that well-organized large coherent structures are present in the regions close to the plume base, while a more disorganized flow field indicating the development of small scales is present at the downstream. In this plot, the high values of enstrophy are prevalent at the downstream, which are associated with the breakdown of large vortical structures into small scales.

From Figs. 1–4, it is also observed that the flow remains symmetric about the geometric center of the plume. This is due to the fact that there was no force to break the flow symmetry in the simulations. To isolate the effects of buoyancy instability from the shear instability, external perturbations were not used at the inflow boundary in this study. This is different from the non-buoyant reactive jet simulations performed by Grinstein and Kailasanath (1995, 1996), in which asymmetric perturbations were applied at the inflow boundary to trigger the shear

Fig. 5. Instantaneous 3D visualization of the vorticity magnitude of the reactive plume at $t = 24.0$.

instability. It is worth noting that the shading of the 3D volume visualization in Fig. 5 depends not only on the quantity magnitude but also on the viewing distance and angle. Although the simulated buoyant reactive flow remains symmetric due to the absence of disturbance, the breakdown of large scale vortices into small scales as that indicated in Fig. 5 still occurs in the flow field due to 3D vortex interactions.

For a diffusion flame, the flow must satisfy two criteria for a significant reaction to occur: both the fuel and oxidizer must be mixed at a given point in the field and the temperature must be high enough at that point. Fig. 6 shows the reaction rate profiles at the centerline of the reactive plume at three different times corresponding to approximately one pulsation period. The periodicity is indicated by the close match of the reaction rates at $t = 22.0$ and $t = 24.0$ as the period of the pulsation is about $\Delta t = 2.0$. In the reactive plume, buoyancy-induced large vortical structures control the mixing process and cause the periodic behavior of the diffusion flame. The flame intermittency associated with the pulsation is also evident in this figure. The formation of the holes inside the flame in which no chemical reactions take place can be attributed to the local unmixedness of the fuel/oxidizer mixture due to the vortical structures and fuel consumption at the downstream.

An important parameter in turbulent combustion modelling is the scalar dissipation rate (Peters, 1984; Bray and Peters, 1994). Many popular turbulent combustion modelling approaches, such as the flamelet models (Peters, 1984), are based on the scalar dissipation rate and assume that the reaction occurs along the stoichiometric surface where the scalar dissipation is intense (Peters, 1984; Bray and Peters, 1994). For a diffusion flame, the mixing process can be represented by the mixture fraction $\xi = (sY_f - Y_o + 1)/(1 + s)$, where $s = (v_o W_o)/(v_f W_f)$ stands for the mass of oxidizer required to react with a unit mass of fuel. The non-dimensional dissipation rate of mixture fraction is defined as $\chi = 2\mu/(ReSc)\nabla\xi \cdot \nabla\xi$. Fig. 7 shows the scalar dissipation rate profiles at the centerline of the non-premixed flame corresponding to the reaction rates shown in Fig. 6. It is observed that there is a rough correspondence between the peaks of scalar dissipation rate and the intense reaction zones. However, the scalar dissipation zones are narrower than the reaction zones. Furthermore, the peaks of scalar dissipation rate lag slightly behind the peaks of reaction rate. Mahalingam et al. (1990) also observed the breakdown of the correspondence between scalar dissipation and intense reaction zones in their simulation of a buoyant diffusion flame, which was explained as a consequence of the buoyancy-induced vortical structures. A more likely reason, however, is that the DNS simulates a more realistic finite-rate chemistry instead of the fast chemistry assumed in turbulent combustion modelling based on χ. The issue clearly needs further investigation.

3.2. Flow transition and vortex dynamics

The underlying fluid dynamics leading to the large and small vortical structures in the reactive plume can be understood by examining the vorticity transport. The trend of the increase of the small scales in the more disorganized downstream portion of

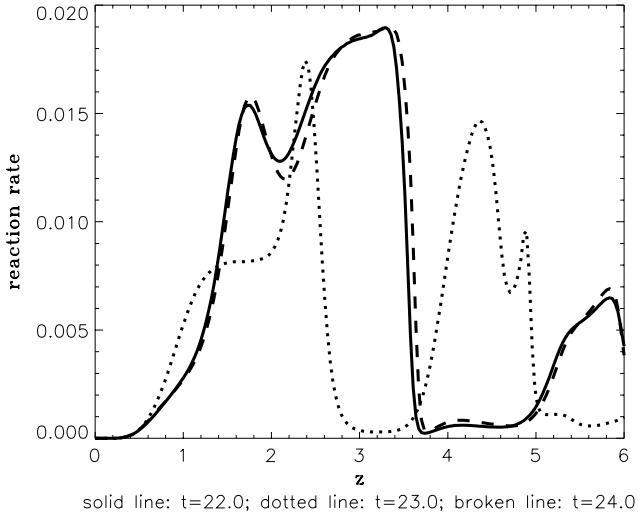

Fig. 6. Reaction rate profiles at the centerline of the reactive plume.

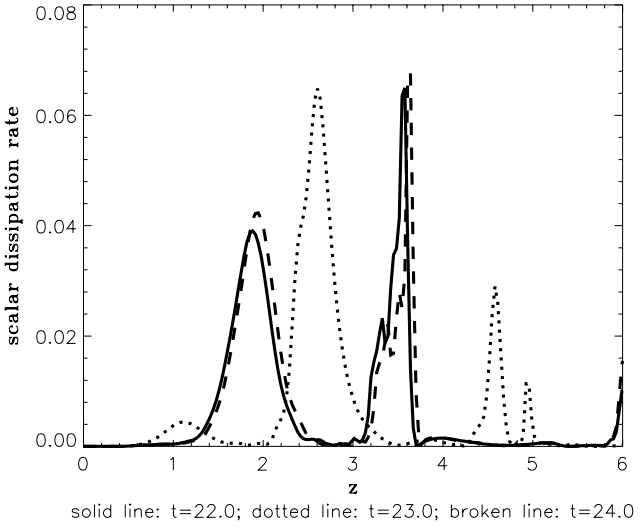

Fig. 7. Scalar dissipation rate profiles at the centerline of the reactive plume.

the reactive plume such as shown in Fig. 5 can be further understood by spectral analysis of the flow field. Fig. 8 shows the energy spectra of the reacting case determined from the history of the instantaneous centerline streamwise velocity at different vertical locations of the flow field by using Fourier analysis, which is expressed in logarithmic scales (to the base 10) of the non-dimensional frequency (Strouhal number) and kinetic energy. The spectral analysis used velocity data taken over a time interval of six pulsation periods for the fully developed reactive plume after the initial stage of the simulation. It can be observed that the most energetic mode occurs at a low frequency, which is about $St = 0.5$. This frequency is the "puffing" or "flickering" frequency of the buoyant reactive plume associated with the formation and convection of large vortical structures in the flow field (Jiang and Luo, 2000a). Further downstream, the flow becomes more energetic, and higher frequency harmonics are developed in the flow field.

The most important feature in Fig. 8 is the development of these high frequency harmonics associated with the popularity of small scales at the downstream of the reactive plume, which indicates the emergence of small-scale turbulence in the flow field. At the location of $z = 6.0$, the centerline streamwise velocity fluctuates approximately between 1.0 and 3.0 with the temperature fluctuating around $T = 2.0$, the local turbulence Reynolds number is roughly estimated to be about 300, which is high enough for turbulence to develop. Flow transition to turbulence is the direct consequence of the breakdown of large scale vortical structures due to strong vortex interactions, especially the interactions between the streamwise vorticity and the cross-streamwise vorticity (Grinstein and DeVore, 1996). The quantitative trends of transition to turbulence can be measured by the Kolmogorov cascade theory, which states a power law correlation between the energy and frequency: $E(St) \sim St^{-5/3}$. In Fig. 8, the Kolmogorov power law is plotted together with the energy spectrum at the location of $z = 6.0$. Apparently the behavior of this rectangular reactive plume follows the Kolmogorov cascade theory, indicating the occurrence of flow transition to turbulence at the downstream.

For comparison, Fig. 9 shows the Fourier analysis of the energy spectra of the instantaneous streamwise velocity at different vertical locations of the non-reactive buoyant thermal plume. This non-reactive plume is less energetic than the reactive plume at small scales, although the puffing or flickering frequencies of the two cases are quite close. The non-reactive thermal plume does not develop significant high frequency harmonics at the downstream, due to the lack of small scales. This is a significant difference between the reactive plume and the non-reactive thermal plume. The non-reactive thermal plume is much less vortical than the reactive plume (as shown in Fig. 4) because of insufficient buoyancy effects, consequently vortex interactions and breakdown do not occur in this non-reactive thermal plume. The results indicate the importance of combustion-induced buoyancy effects on the flow transitional dynamics.

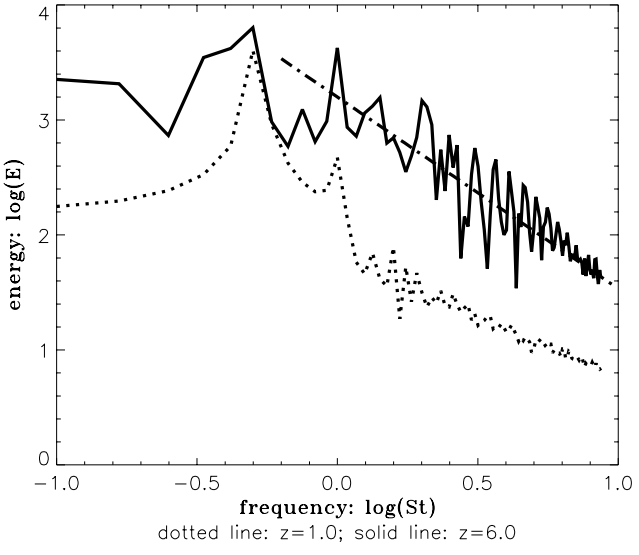

Fig. 8. Energy spectra of the instantaneous centerline velocity at different vertical locations of the reactive plume (chained line: Kolmogorov cascade theory $\sim St^{-5/3}$).

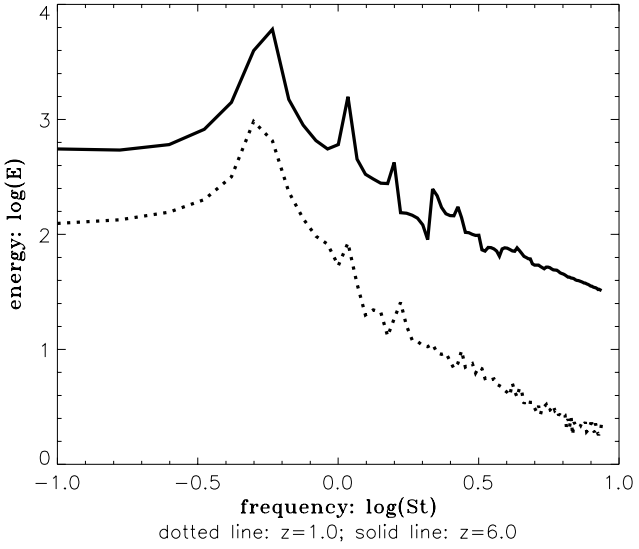

Fig. 9. Energy spectra of the instantaneous centerline velocity at different vertical locations of the thermal plume.

For non-buoyant reactive jets, Grinstein and Kailasanath (1995, 1996) found that the effect of chemical heat release was to reduce the flow vortical level and relaminarize the turbulent flow field. In their simulations, the non-buoyant jets were perturbed at the inflow boundary to trigger the flow turbulent behavior. For the buoyant cases studied here, simulations performed without external disturbance indicate that the vortical structures due to buoyancy are self-sustaining. In contrast with the relaminarization effects of chemical exothermicity on non-buoyant jets, the combustion-induced buoyancy in the reactive plume enhances the flow vortical level and the tendency towards transition to turbulence. The mechanism behind this is that buoyancy has the effect of promoting the flow vortical level as discussed below.

Vorticity is a transportable quantity and, once generated, it can be convected, diffused, augmented or terminated. The governing equation for the vorticity transport in buoyant flows with gravitational effect can be written in a vector form as

$$\frac{D\boldsymbol{\omega}}{Dt} = (\boldsymbol{\omega}\cdot\nabla)\mathbf{V} - \boldsymbol{\omega}(\nabla\cdot\mathbf{V}) + \frac{1}{\rho^2}(\nabla\rho\times\nabla p) + \frac{1}{\rho^2}\frac{\rho_a}{Fr}(\nabla\rho\times\mathbf{g}) + \nabla\times\left(\frac{1}{\rho}\nabla\cdot\boldsymbol{\tau}\right). \quad (3)$$

The terms on the right-hand side are the vortex stretching term, dilatation term, baroclinic torque, gravitational term, and viscous term, respectively. Among the five terms on the right-hand side of Eq. (3), it is known that the dilatation term and viscous term mainly attenuate flow vorticity (Givi, 1989). The relaminarization effect of chemical heat release on non-buoyant jet flames such as that observed by Grinstein and

Kailasanath (1995, 1996) is mainly because of these two terms (Jiang and Luo, 2000b). However, the importance of these two terms in the vorticity transport budget is insignificant for buoyant flows with moderately high Reynolds number and low Froude number (Jiang and Luo, 2000a,b,c), such as the case investigated here.

For buoyant flows, the stretching term, baroclinic torque and gravitational term are the major terms in the vorticity transport. It was identified that the combined effect of these terms is to promote the flow vortical level of buoyant jets and plumes (Jiang and Luo, 2000a,b,c). Among the major terms, the gravitational term promotes the flow vortical level not only in a global sense but also in a local sense, while the baroclinic torque can either promote or destroy vorticity depends on the local flow structures. The stretching term spatially distributes the vorticity in three dimensions.

In most cases, the gravitational term due to the interaction between density gradients and gravity is an important term in the vorticity generation of buoyant jets and plumes, which can initiate flow vorticity (Jiang and Luo, 2000a,b,c). The gravitational term is zero for non-buoyant jets, but it is significant for buoyant flows. The three components of the gravitational term in general form are $\rho_a(g_z\partial\rho/\partial y - g_y\partial\rho/\partial z)/(\rho^2 Fr)$, $\rho_a(g_x\partial\rho/\partial z - g_z\partial\rho/\partial x)/(\rho^2 Fr)$, and $\rho_a(g_y\partial\rho/\partial x - g_x\partial\rho/\ \partial y)/(\rho^2 Fr)$, in x, y, and z directions, respectively. For the flow configuration in this study, they are $-\rho_a\partial\rho/\partial y/(\rho^2 Fr)$, $\rho_a\partial\rho/\partial x/(\rho^2 Fr)$, and 0, respectively. This implies that the gravitational term does not contribute to the streamwise vorticity. However, once the cross-streamwise vorticity ω_x and ω_y are generated, the significant vortex stretching $\omega_x\partial w/\partial x + \omega_y\partial w/\partial y + \omega_z\partial w/\partial z$ and baroclinic torque $(\partial\rho/\partial x\partial p/\partial y - \partial\rho/\partial y\partial p/\partial x)/\rho^2$ in the streamwise direction will subsequently lead to the development of streamwise vorticity. For brevity, the detailed transport budgets are not shown here.

For the reacting case, combustion leads to high temperatures, and in turn higher density inhomogeneities in the flow field compared with the non-reactive case. Due to the more significant gravitational effects, vortex stretching, and baroclinic torque, the reactive flow field is much more vortical than the non-reactive thermal plume, and therefore it has a strong tendency of transition to turbulence under the effects of combustion-induced buoyancy.

Fig. 10 shows the history of the vorticity extrema in the computational domain of the rectangular reactive plume. The streamwise vorticity ω_z is initially zero, it develops after the development of the vorticity in the cross-stream directions. When the flow reaches the periodic stage, the streamwise vorticity is about the same amplitude as the cross-streamwise vorticity ω_x in the minor axis direction. With the spatial development of the reactive plume, strong 3D vortex interactions occur at the downstream of the flow field due to the development of the significant streamwise vorticity. These interactions consequently lead to the breakdown of the large scale vortical structures, and mixing transition (Dimotakis, 2000) occurs as shown in Fig. 8 by the energy spectrum at the downstream of the reactive flow field. From Fig. 10, it also can be observed that the vorticity in the major axis direction ω_y is higher (in terms of absolute value) than that of the vorticity in the minor axis direction ω_x due to the aspect ratio effect of the rectangular geometry.

3.3. Time-averaged flow quantities

Simulation results presented above are instantaneous quantities. Time-averaged flow statistics are also of interests. Mean global plume properties were obtained by averaging the flow quantities over six pulsation periods after the initial transients had been convected out of the computational domain. Figs. 11 and 12 show the streamwise velocity distributions of the rectangular reactive plume.

For the mean flow field of non-circular jets, the most interesting discovery was the phenomenon of axis-switching (Ho and Gutmark, 1987; Gutmark and Grinstein, 1999). Jet spreading in the minor axis plane was observed to be much greater than that in the major axis plane. This has been understood as the consequence of the vortex deformation and self-induction processes associated with the aspect ratio and corner effects of non-circular jets (Grinstein and DeVore, 1996; Wilson and Demuren, 1998; Gutmark and Grinstein, 1999). Up to date, reports on the near field mean flow characteristics of buoyant non-circular jets and plumes are very scarce. The averaged quantities presented in Figs. 11 and 12 reveal the effects of buoyancy on the mean flow quantities in the near field.

The time-averaged streamwise velocity profiles on the major and minor axis planes of the reactive plume are shown in Figs. 11 and 12, respectively. It can be seen that the reactive

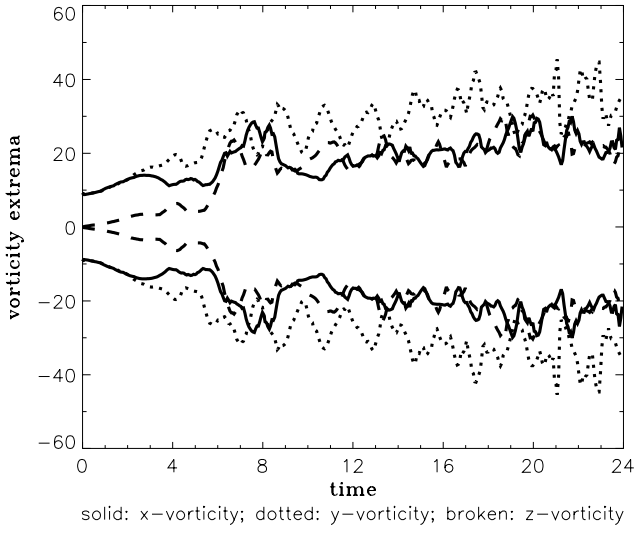

Fig. 10. History of the vorticity extrema of the reactive plume.

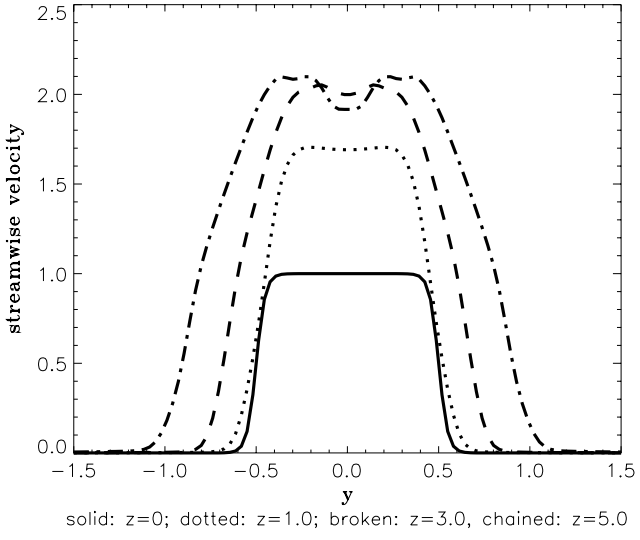

Fig. 11. Time-averaged streamwise velocity profiles on the major axis plane of the reactive plume.

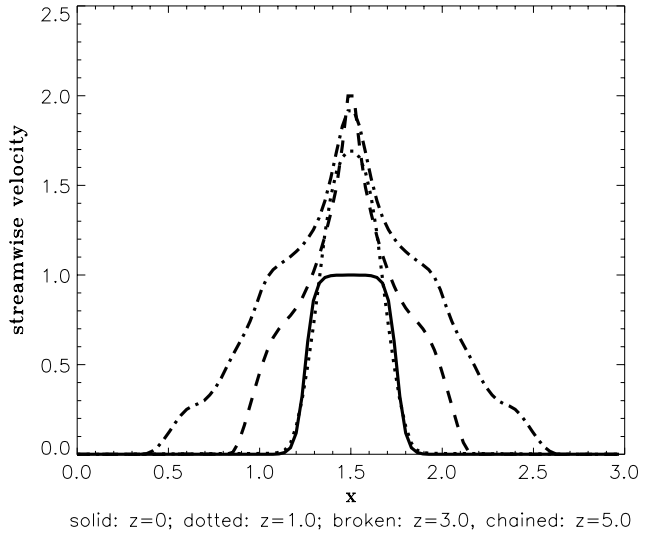

Fig. 12. Time-averaged streamwise velocity profiles on the minor axis plane of the reactive plume.

plume grows much faster in the minor axis direction than in the major axis direction at the downstream. The plume spreading in the minor axis direction is almost twice as fast as that in the major axis. This trend is similar to that observed for non-buoyant jets. It is evident that this plume has a tendency towards axis-switching similar to that observed for non-buoyant jets. This is due to the fact that the vortex deformation effects due to 3D vortex interactions also occur in this buoyant plume although the mechanisms leading to the formation of vortices in plumes and non-buoyant jets differ from each other. The results shown indicate the aspect ratio and corner features of the rectangular buoyant reactive plume.

From Figs. 11 and 12, it is observed that within the distance of $z = 1.0$, the plume does not spread in both the major and minor axis directions, but the streamwise velocity increases significantly within this distance. It is because of the buoyancy acceleration and the necking phenomenon close to the inlet plane as those shown in the instantaneous plots. This trend is different from that reported for non-buoyant jets (Ho and Gutmark, 1987), in which the averaged velocity decays in the streamwise direction with the jet spreading in lateral directions. At this distance, the flow also maintains its top-hat profile specified at the inlet. The situation is quite different further downstream. The flow acceleration decays in the streamwise direction with the progress of the mixing. The mixing process is dominated by the vortical structures due to combustion-induced buoyancy effects, and the breakdown of vortices due to 3D vortex interactions at the downstream has a significant impact on the mixing process. It can be observed that the centerline velocity at $z = 5.0$ is slightly lower than that at $z = 3.0$ with the spreading of the plume in lateral directions. It is worth noting that there is no comparable experimental data available, and thus, a direct comparison with experiments is not feasible.

4. Summary and conclusions

The near field dynamics of buoyant jets and plumes, including flow instabilities, formation and interaction of the large scale vortical structures and flow transition to turbulence, is an area requiring a better understanding. Although spatial DNS of non-circular jet flames are available in the literature, this study is the first attempt to investigate the near field dynamics of non-circular jet diffusion flames under the effects of buoyancy.

The dynamics of buoyancy-driven non-circular jet diffusion flames mainly depends on the buoyancy instability which is different from that of non-buoyant jet diffusion flames. In buoyant diffusion flames, formation and convection of the buoyancy-induced vortical structures lead to the periodic behavior of the flame in the near field. The large scale vortical structures facilitate the mixing between the fuel and oxidizer. These large vortical or coherent structures also interact with the reaction zone, thereby causing periodic distortions of the reaction zone, oscillations of the flame temperature and thickness. The flame shows discontinuity and non-uniformity due to the existence of the large vortical structures.

A strong tendency towards flow transition to turbulence due to the combustion-induced buoyancy effects has been observed for the rectangular reactive plume. In the regions close to the inlet, formation of the large coherent structures and the necking phenomenon due to buoyancy effects are observed. As the flow develops spatially in the streamwise direction, a more disorganized flow regime appears at the further downstream, characterized by smaller scales indicating the development of turbulence in the flow field. The energy spectrum of the instantaneous velocity at the downstream of the reactive plume is consistent with the Kolmogorov cascade theory. The breakdown of the vortices and flow transition are the consequences of 3D vortex interactions. Unlike non-buoyant jet diffusion flames, the transition in the rectangular buoyant diffusion flame develops naturally without applying external perturbations at the flow boundary. This has been understood as the consequence of the combustion-induced buoyancy effects.

For the averaged flow quantities, unlike the decay of the streamwise velocity of non-buoyant jets, the streamwise velocity of the buoyant reactive plume increases at locations very close to the plume base, while it starts to decay at the downstream with further mixing of the fluid due to turbulence. The corner and aspect ratio effects of non-circular jets are also observed in this rectangular buoyant reactive plume, which has the tendency towards axis-switching.

Acknowledgements

This work was funded by the UK Engineering and Physical Sciences Research Council under grant No. GR/L67271.

References

Bray, K.N.C., Peters, N., 1994. Laminar flamelets in turbulent flames. In: Libby, P.A., Williams, F.A. (Eds.), Turbulent Reacting Flows. Academic Press, London, pp. 63–113.

Candel, S., Thevenin, D., Darabiha, N., Veynante, D., 1999. Progress in numerical combustion. Combust. Sci. Technol. 149, 297–337.

Cetegen, B.M., Ahmed, T.A., 1993. Experiments on the periodic instability of buoyant plumes and pool fires. Combust. Flame 93, 157–184.

Cetegen, B.M., Dong, Y., Soteriou, M.C., 1998. Experiments on stability and oscillatory behavior of planar buoyant plumes. Phys. Fluids 10, 1658–1665.

Dimotakis, P.E., 2000. The mixing transition in turbulent flows. J. Fluid Mech. 409, 69–98.

Elghobashi, S., Zhong, R., Boratav, O., 1999. Effects of gravity on turbulent nonpremixed flames. Phys. Fluids 11, 3123–3135.

Givi, P., 1989. Model-free simulations of turbulent reactive flows. Prog. Energy Combust. Sci. 15, 1–107.

Grinstein, F.F., DeVore, C.R., 1996. Dynamics of coherent structures and transition to turbulence in free square jets. Phys. Fluids 8, 1237–1251.

Grinstein, F.F., Kailasanath, K., 1995. Three-dimensional numerical simulations of unsteady reactive square jets. Combust. Flame 100, 2–10.

Grinstein, F.F., Kailasanath, K., 1996. Exothermicity and relaminarization effects in unsteady reactive square jets. Combust. Sci. Technol. 114, 291–312.

Gutmark, E.J., Grinstein, F.F., 1999. Flow control with noncircular jets. Annu. Rev. Fluid Mech. 31, 239–272.

Hertzberg, J.R., Ho, C.M., 1995. Three-dimensional vortex dynamics in a rectangular sudden expansion. J. Fluid Mech. 289, 1–27.

Ho, C.M., Gutmark, E.J., 1987. Vortex induction and mass entrainment in a small-aspect-ratio elliptic jet. J. Fluid Mech. 179, 383–405.

Huerre, P., Monkewitz, P.A., 1990. Local and global instabilities in spatially developing flows. Annu. Rev. Fluid Mech. 22, 473–537.

Jiang, X., Luo, K.H., 2000a. Direct numerical simulation of the puffing phenomenon of an axisymmetric thermal plume. Theoret. Comput. Fluid Dynamics 14, 55–74.

Jiang, X., Luo, K.H., 2000b. Spatial direct numerical simulation of the large vortical structures in forced plumes. Flow Turbulence Combust. 64, 43–69.

Jiang, X., Luo, K.H., 2000c. Combustion-induced buoyancy effects of an axisymmetric reactive plume. Proc. Combust. Inst. 28, 1989–1995.

Katta, V.R., Goss, L.P., Roquemore, W.M., 1994. Numerical investigations of transitional H_2/N_2 jet diffusion flames. AIAA J. 32, 84–94.

Lele, S.K., 1992. Compact finite difference schemes with spectral-like resolution. J. Comput. Phys. 103, 16–42.

Lingens, A., Reeker, M., Schreiber, M., 1996. Instability of buoyant diffusion flames. Exp. Fluids 20, 241–248.

Luo, K.H., 1999. Combustion effects on turbulence in a partially premixed supersonic diffusion flame. Combust. Flame 119, 417–435.

Luo, K.H., Bray, K.N.C., 1998. Combustion-induced pressure effects in supersonic diffusion flames. Proc. Combust. Inst. 27, 2165–2171.

Mahalingam, S., Cantwell, B.J., Ferziger, J.H., 1990. Full numerical simulation of coflowing axisymmetric jet diffusion flames. Phys. Fluids 2, 720–728.

Maxworthy, T., 1999. The flickering candle: transition to a global oscillation in a thermal plume. J. Fluid Mech. 390, 297–323.

Miller, R.S., Madnia, C.K., Givi, P., 1995. Numerical simulation of non-circular jets. Comput. Fluids 24, 1–25.

Moin, P., Mahesh, K., 1998. Direct numerical simulation: a tool in turbulence research. Annu. Rev. Fluid Mech., 30,539–578.

Peters, N., 1984. Laminar diffusion flamelet models in non-premixed turbulent combustion. Prog. Energy Combust. Sci., 10,319–339.

Poinsot, T.J., Lele, S.K., 1992. Boundary conditions for direct simulations of compressible viscous flows. J. Comput. Phys. 101, 104–129.

Thompson, K.W., 1987. Time dependent boundary conditions for hyperbolic systems. J. Comput. Phys. 68, 1–24.

Vervisch, L., Poinsot, T., 1998. Direct numerical simulation of non-premixed turbulent combustion. Annu. Rev. Fluid Mech. 30, 655–691.

Williamson, J.H., 1980. Low-storage Runge–Kutta schemes. J. Comput. Phys. 35, 48–56.

Wilson, R.V., Demuren, A.O., 1998. Numerical simulation of turbulent jets with rectangular cross-section. ASME J. Fluids Eng. 120, 285–290.

Zhang, X., 2000. Turbulence measurements of an inclined rectangular jet embedded in a turbulent boundary layer. Int. J. Heat Fluid Flow 21, 291–296.